Lawrence Berkeley National Laboratory

Title

Additive Lithography—Organic Monolayer Patterning Coupled with an Area-Selective Deposition

Permalink

https://escholarship.org/uc/item/1t52q47w

Journal

ACS Applied Materials & Interfaces, 13(7)

ISSN

1944-8244

Authors

Wojtecki, Rudy
Ma, Jonathan
Cordova, Isvar
et al.

Publication Date

2021-02-24

DOI

10.1021/acsami.0c16817

Peer reviewed

Additive Lithography – Organic Monolayer Patterning Coupled with an Area Selective Deposition

Rudy Wojtecki[†*], Jonathan Ma[§], Isvar Cordova[§], Noel Arellano[†], Krystelle Lionti[†], Teddie Magbitang[†], Thomas G. Pattison[§§], Xiao Zhao[††‡‡], Eugene Delenia[†], Nicholas Lanzillo[‡], Alexander E. Hess[†], Noah Fine Nathel[†], Holt Bui[†], Charles Rettner[†], Gregory Wallraff[†] and Patrick Naulleau[§]

† International Business Machines - Almaden Research Center, 650 Harry Rd., San Jose, CA 95110, USA
‡ International Business Machines - Semiconductor Technology Research, 257 Fuller Rd., Albany, NY 12203, USA
§ Center for X-ray Optics, Materials Science Division, Lawrence Berkeley National Laboratory, 1 Cyclotron Rd., Berkeley, CA 94720
† † Materials Sciences Division, Lawrence Berkeley National Laboratory, Berkeley, California, 94720, United States
‡ ‡ Department of Materials Science and Engineering, University of California at Berkeley, Berkeley, California 94720, United States
§§ Polymer Science Group, Department of Chemical Engineering, The University of Melbourne, Parkville, VIC 3010, Australia

* Corresponding Author: rjwojtec@us.ibm.com

ORCID:
Rudy Wojtecki - https://orcid.org/0000-0003-0967-5007
Alexander Hess - https://orcid.org/0000-0002-3227-700X
Thomas Pattison - http://orcid.org/0000-0002-3029-5896
Noah Fine Nathel - https://orchid.org/0000-0001-7628-8803
Isvar Cordova - https://orcid.org/0000-0003-0800-9301
Jonathan Ma - https://orcid.org/0000-0001-8936-4035

Keywords – Atomic Layer Deposition, Area Selective Deposition, Self-Assembled Monolayers, Nanolithography, Photocrosslinking

Abstract

The combination of area selective deposition (ASD) with a patternable

organic monolayer provides a versatile additive lithography platform,

enabling the generation of a variety of nanoscale feature geometries.

Stearate hydroxamic acid self-assembled monolayers (SAM) were patterned

with extreme ultraviolet (λ=13.5 nm) or electron beam irradiation and

developed with ASD to achieve line space patterns as small as 50nm.

Density functional theory (DFT) was employed to aid in the synthesis of

1

hydroxamic acid derivatives with optimized packing density to enhance imaging contrast and improve dose sensitivity. Near edge x-ray absorption fine structure spectroscopy and infrared spectroscopy reveals the imaging mechanism is based on improved deposition inhibition provided by the crosslinking of the SAM, to produce a more effective barrier during a subsequent deposition step. With patterned substrates composed of co-planar copper lines and silicon spacers, hydroxamic acids selectively formed monolayers on the metal portions and could undergo a pattern-wise exposure followed by ASD in the first combination of a patternable monolayer with ASD. This materials system presents an additional capability compared to traditional ASD approaches that generally reflect a starting patterned surface. Furthermore, this bottoms-up additive approach to lithography may be a viable alternative to subtractive nanoscale feature generation.

Introduction

The design of photo-responsive materials for the controlled generation of patterns drives device miniaturization and has broad reaching applications in computing, biomedical,[1] sensors[2,3] and catalysis[4] that extend human capabilities. The performance demands for patterning materials are ever increasing across technological platforms – from the ability resolve ever smaller critical dimensions for the fabrication of semiconductor devices[5] to the chemical control over surface functional groups for biological sensors[6,7,8] and diagnostic tools[9]. Current approaches to nanoscale fabrication are

2

reliant on subtractive processes to pattern materials. However, the subtraction of a material often alters the chemical composition of a surface (such as oxidation) and can damage the material by amorphizing the sidewalls of an otherwise crystalline thin film, from reactive ion etching or solution-based chemical etches, for instance.[10] As device dimensions continue to undergo miniaturization to single nanometer regimes, surfaces and interfaces become increasingly significant and can dominate the performance of a final device. However, an 'additive strategy' to nanoscale patterning where a film is 'added' in a selected area, versus 'subtracted', presents a pathway for a fundamental alternative approach to nanofabrication, where one may grow a device without damage to surfaces or interfaces using 'additive lithography.' This approach is demonstrated with photosensitive monolayers which, after pattern-wise irradiation crosslink the material, generating a selective barrier that guides the film growth of a metal oxide to achieve high fidelity patterns and demonstrated on features as small as 50 nm.

Area selective depositions (ASD) are garnering increased attention for their potential to simplify fabrication process flows and address overlay errors for conventional lithography in the near term and wider ranging applications in the future.[11,12,13,14] These processes generally require pre-patterned surfaces composed of dissimilar materials, copper and silicon, for instance, where surface reactivity or the addition of an inhibiting material is exploited to block deposition on one surface and enabling (or promoting)

growth on another. For instance, the selective deposition of TiO_2 can be

achieved on an oxide surface and growth inhibited on a hydrogen terminated

one.[15] There are, of course, a variety of methods to enable ASD, such as

exploiting differences in surface reactivity,[11] the use of conventional resist

materials,[16] amorphous carbon[1718] and other small molecules.[19,20] However,

self-assembled monolayers (SAMs) exhibit some of the highest levels of

selectivity.[21,22,23,24,25,26,27] SAMs are a distinct class of organic material that

assemble from the surface adsorption and orientation of small molecules

that form well-ordered crystalline monolayers.[28] SAM constituents are

composed of a head group that interacts with the substrate, a tail group that

presents a chemical functional group at the monolayer surface, and the side-

chain – the region between the monolayer surface and the substrate-

anchoring head group. By tailoring the side-chain and tail group SAMs can

operate in either capacity to inhibit or activate selected regions from

deposition.[15,16,29,30,31] By careful selection of the head group SAM formation

can be self-aligning, for example in the use of alkyl phosphonates, as they

preferentially form on a metal (or metal oxide) surface and not on a silicon or

silicon dioxide surface. This selective SAM formation therefore occurs

without a patterning step and therefore without the need to have a

mask/pattern alignment step to the underlying pre-pattern, as would be

typically required in depositing most other materials at a surface. Once the

SAM is deposited the surface is deactivated during the self-limiting ALD half

reactions, where the SAM protects a chemically reactive surface by blocking

4

the adsorption of ALD reagents enabling deposition to only occur on a desired portion of the substrate – where little or no inhibitor is present (**Figure 1**).[32] Therefore, monolayer coverage, density and spacing between components are critical parameters to achieve effective inhibition (though the impact of monolayer ordering on inhibition is not as clear, as both amorphous and crystalline materials are capable of inhibiting film growth[33]). This method to localize deposition is, however, primarily limited to creating surface topography reflecting the underlying pre-pattern.[34,35,36]

An example of additive lithography is presented that describes the combination of a patternable self-assembled organic monolayer (SAM) with ASD to grow a patterned film in an additive approach. During a pattern-wise exposure, the monolayer undergoes a chemical transformation to crosslink the SAM, which deactivates the selected region towards atomic layer deposition (ALD). This exposure induced inhibition strategy was employed to selectively grow ALD films in unexposed regions and inhibit growth in exposed regions to produce relief images with thickness differences as much as 35nm. In this fashion ALD is used to "develop" the relief image from the chemical differences in a monolayer created from a pattern-wise exposure (**Figure 1**). This patterning material can be combined with its selective attachment to a metal portion of a prepatterned surface where a subsequent exposure can be used to inhibit ALD film formation on localized regions of the metal surface with deposition then occurring on both the dielectric surface and unexposed SAM surface. The ALD growth rate on these surfaces

5

may vary though, as the unexposed portion of the SAM will delay film growth a longer number of cycles compared to the dielectric surface and therefore may result in a difference in deposited film thickness on the two surfaces.
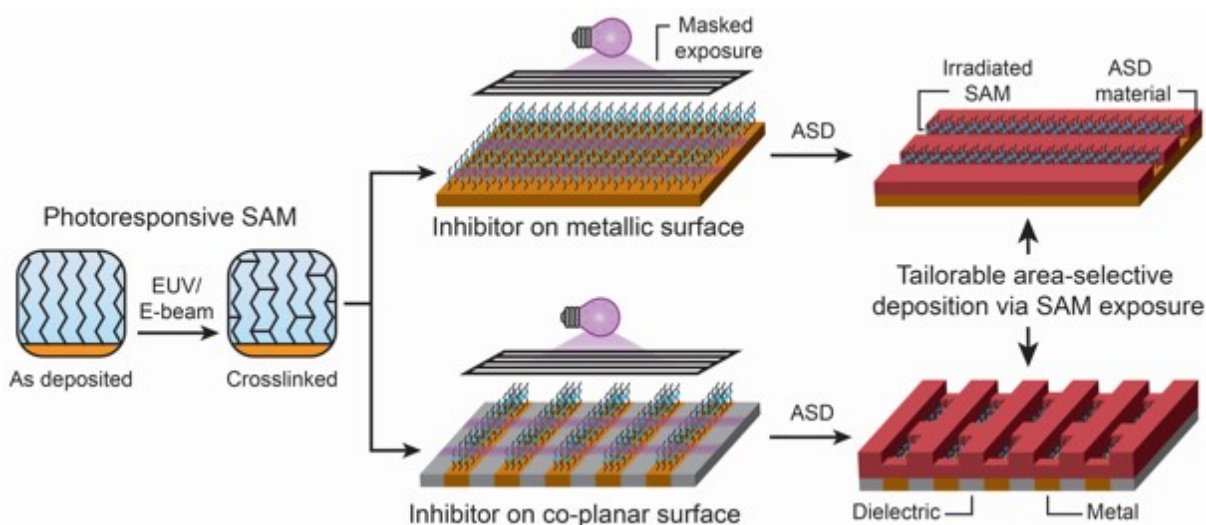

Figure 1: Schematic representation of a patternable self-assembled monolayer (SAM) that undergoes crosslinking upon exposure to either extreme ultraviolet (EUV) or electron beam irradiation. (top) A blanket metal thin film coated with patternable SAM undergoes a patterned exposure followed by an area selective deposition (ASD) where a film is generated selectively from the surface of the unexposed SAM. (bottom) On a patterned surface (metal lines and silicon spaces) a patternable SAM selectively forms on the metal and can undergo patterning followed by ASD to selectively grow a film on the silicon surface as well as the unexposed regions of the SAM.

Results and Discussion

Self-Assembled Monolayers Based on Hydroxamic acids

High-resolution imaging systems typically rely on the ability to produce non-linear responses during image generation (e.g., high-contrast imaging). For instance, Chemically Amplified Resists (CARs), the mainstay of high-

6
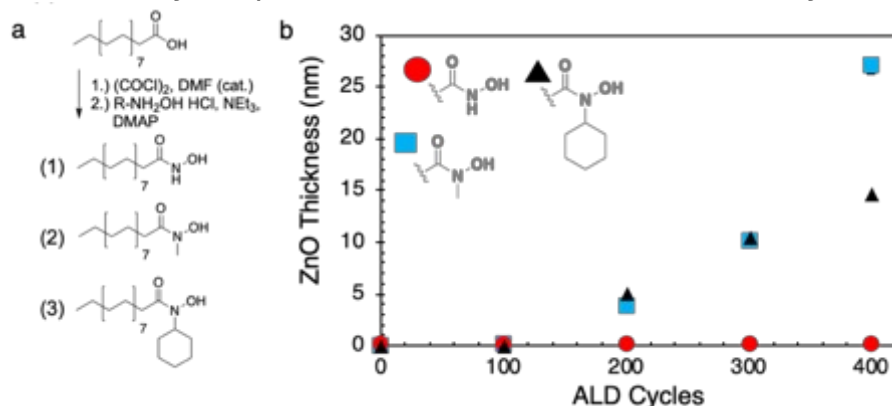
performance patterning, rely on a photo-stimulus to trigger a chemical reaction and a feedback loop, amplifying the concentration of polar moieties from a single photolysis event.[37] This patternable monolayer system takes advantage of the ALD process to build contrast, instead of the exposure induced chemistry itself. In this system contrast can be enhanced by the use of different SAM materials to adjust the interactions or spacing between components. A material platform that affords a synthetic handle to provide this intermolecular control are hydroxamic acid based SAMs, where substituents can be introduced at the head group through facile synthetic methods.

Scheme 1: Synthesis of Hydroxamic Acids and SAM Based Inhibition
(**a**) Synthesis of hydroxamic acid monolayer components with increasing head group substituents (1) -H (2) -CH$_3$ (3) -C$_6$H$_{11}$. (**b**) Inhibition properties of SAMs produced from (1), (2) and (3) after the atomic layer deposition of ZnO as measured by Rutherford Backscattering with a standard measurement error of 3% of the film thickness.


For this study hydroxamic acids were prepared from stearic acid through a simple two step method where first the acid is activated by the preparation of the corresponding acyl chloride, followed by the addition of the corresponding hydroxyl amine (**Scheme 1**). Where the octadecyl- (C$_{18}$) moiety was selected as it acts as an effective inhibitor in the ALD of metal oxides.[38]

Each hydroxamic acid derivative produces hydrophobic monolayer films on metal (copper used in studies) or metal oxide surfaces, from an immersion and rinse process, where the monolayers produced static water

contact angles between 70-110° consistent with the formation of hydrophobic surfaces (**Figure S2**). Furthermore, characterization of the monolayer films by FT-IR exhibits a characteristic peak at 2920 cm^{-1} corresponding with the C-H stretch which is sharp and well defined (full width at half maximum, FWHM, ca. 40 cm^{-1}) consistent with an oriented aliphatic chain with a low number of trans-gauche packing defects consistent with a well-ordered monolayers, by comparison a broad peak at this location (FWHM $\geq$ 100 cm^{-1}) would indicate a disordered monolayer (**Figure S3**).[39]

Hydroxamic acid (**1**) readily produces a SAM on a copper thin film and can inhibit more than 400 cycles of ZnO ALD (from half-cycles of diethyl zinc and water at 150°C), as characterized with particle induced x-ray emission (PIXE) and Rutherford Backscattering (RBS). Both PIXE and RBS are non-destructive characterization methods to measure film thicknesses, composition and stoichiometry of thin films.[40] As the number of ALD cycles are further increased, a film rapidly forms – after 600 cycles a 15nm film was measured, compared to 24nm on an uninhibited surface (**Figure S1**). The substituted monolayers (**2**) and (**3**) in response to ALD show significantly lower ALD inhibition (e.g., 100 cycles) compared to (**1**), consistent with either decreased intermolecular interactions or increased spacing between components.

8

Substituents at hydroxamic acid headgroup of varying size (e.g., -H, -CH$_3$, & -C$_6$H$_{10}$) have a direct impact on the packing characteristics of monolayer components, as shown by DFT calculations (**Figure 2**). Each hydroxamic acid derivative was found to bind strongly to metal surfaces and
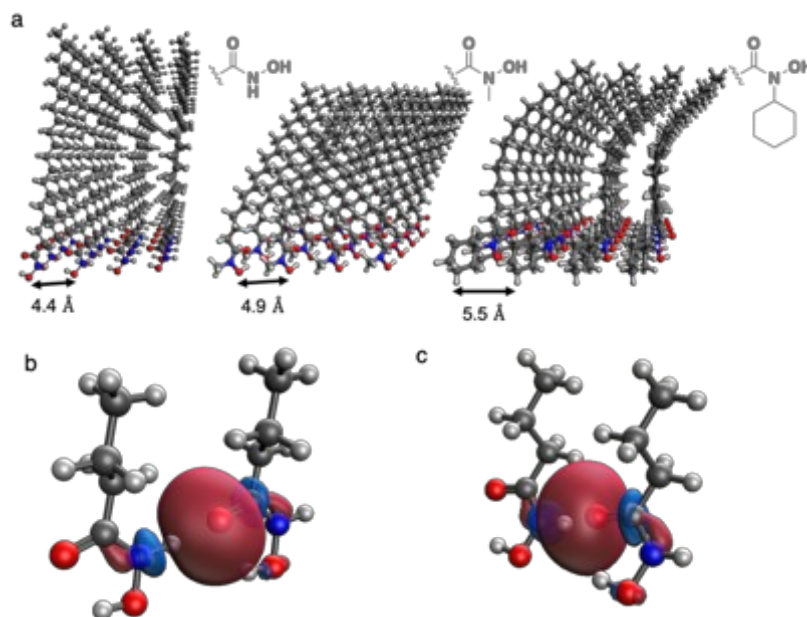
the head group substituents were found to affect binding geometries, which

Figure 2: DFT Modeling of Hydroxamic Acid SAMs (**a**) unit cells highlighting packing density as a function of substituent where with SAM produced from (1) with component spacing of 4.4 Å SAM from (2) with component spacing 4.9 Å and SAM from (3) with 5.5 Å component spacing. (**b**) Visualized localized electron density of orbitals between H(-N) and O(=C) of neighboring molecules indicative of hydrogen bonding.

change the conformation of the headgroup in its interaction with a surface.

For instance, (**1**) produces the most energetically stable conformation in an

out of plane geometry (**Figure 2**). In this configuration, the tilt angle of the

tail normal to the surface is small and component spacing was found to be

4.4 Å. Monolayers with methyl- substituent (**2**) reduces packing

9

density slightly to 4.9 Å between components, while the tail become tilted. This is consistent with literature reports that show SAMs adjust their tilt angle to maximize intermolecular interactions.[41,42] Cyclohexyl derivative (**3**), somewhat unexpectedly, results in the aliphatic chains bending attributed to the slightly sparser packing as component spacing increases to 5.5 Å. The steric repulsion between the cyclohexyl moiety of (**3**) and neighboring hydroxamic acids push components away from neighboring aliphatic chains, straightening the chain, while Van der Waal's interactions pull the tails towards each other. These two competing forces result in bent aliphatic chains. At the optimal geometry, the unit cell of unsubstituted hydroxamic acid (**1**) occupies ca. 19 $Å^2$ while, (**2**) 23 $Å^2$ and (**3**) 30 $Å^2$.

By modeling clusters of (**1**) where they are extracted, truncated in length and assembled in 1x2, 2x2 and 3x3 super cells DFT calculations also indicate hydrogen bonding occurs between neighboring components of (**1**) from interactions of the carbonyl groups and hydroxamic acid protons. Canonical orbitals were extracted and used for localization. Occupied orbitals are localized by Pipek-Mezey method.[43] Localized electron density was identified between H(-N) and O(=C) of neighboring molecules of (**1**). The bonding nature of the localized orbitals is indicative of hydrogen bonding and may be correlated with its greater ALD inhibitory properties compared to derivatives (**2**) and (**3**) that do not contain the H(-N) hydrogen bonding donor.

Inhibition Enhancement of Irradiated Hydroxamic Acid SAMs

10

SAMs produced from hydroxamic acid derivatives underwent open frame Extreme Ultraviolet (EUV, λ=13.5nm) exposures, where 1 cm^2 square areas are subjected to doses ranging from 15 – 215 mJ cm^{-2}. After irradiation, films then underwent ALD with the number of deposition cycles incremented. The exposed and unexposed regions of SAMs were characterized with RBS and PIXE to measure ALD film thickness. After a 215 mJ cm^{-2} EUV exposure dose the SAM produced from (**1**) was found to inhibit 700 ALD cycles (without film formation), versus 500 ALD cycles on unexposed regions (**Figure S1**). After 700 cycles, 35nm of an ALD film was deposited on the unexposed monolayer and no deposition occurred on the exposed regions. Similarly, the exposure of SAMs produced from (**2**) and (**3**) with a 215 mJ cm^{-2} dose exhibited enhanced inhibition preventing film formation up to 500 and 400 cycles, respectively, from 200 cycles without exposure. After 400 cycles 35nm were deposited on unexposed regions of SAMs produced from (**2**) and 15nm with (**3**), without deposition on the exposed regions.

Hydroxamic acid SAMs also exhibited a dose dependence on inhibiting film growth. SAMs produced from (**1**) required a dose at or above 100 mJ cm^{-2} to further improve inhibtion, where ALD film thickness was observed to decrease (**Figure 3**). SAMs produced from substituted hydroxamic acids required lower doses to improve inhibition, where a reduction in film thickness was observed with 35 mJ cm^{-2}, after 400 ALD cycles. Further characterization (described in the next section) reveals irradiation induced chemistry is confined to the crosslinking of the aliphatic moiety of the SAM.

11

Given that all hydroxamic acids used in these studies employ the same aliphatic moiety it is unlikely that the head group modifies the sensitivity of the crosslinking reaction between aliphatic chains (e.g., C-H bond strength is not modified by packing density). This instead would suggest irradiation induced crosslinking significant enhancement to the inhibition of an otherwise poorly inhibiting material such as SAMs produced from (**2**) and (**3**) where potentially low crosslink density significantly enhances inhibition. Whereas further enhancement of an already effective inhibitor, such as (**1**), may not be observed unless more extensive crosslinking occurs.

In control studies SAMs produced from octadecylphosphonic acid and octadecane thiol were evaluated which also employ the same octadecyl-aliphatic chains but vary the head-group (**Figure 3**). In open frame EUV exposures and up to 400 ALD cycles, no deposition occurred in either the exposed or unexposed regions of octadecylphosphonic acid and only a slight difference in Zn surface concentration was observed by x-ray photoelectron spectroscopy (XPS) at the highest EUV dose of 215 mJ cm^{-2} . This further highlights the unique behavior observed with hydroxamic acid based SAMs.
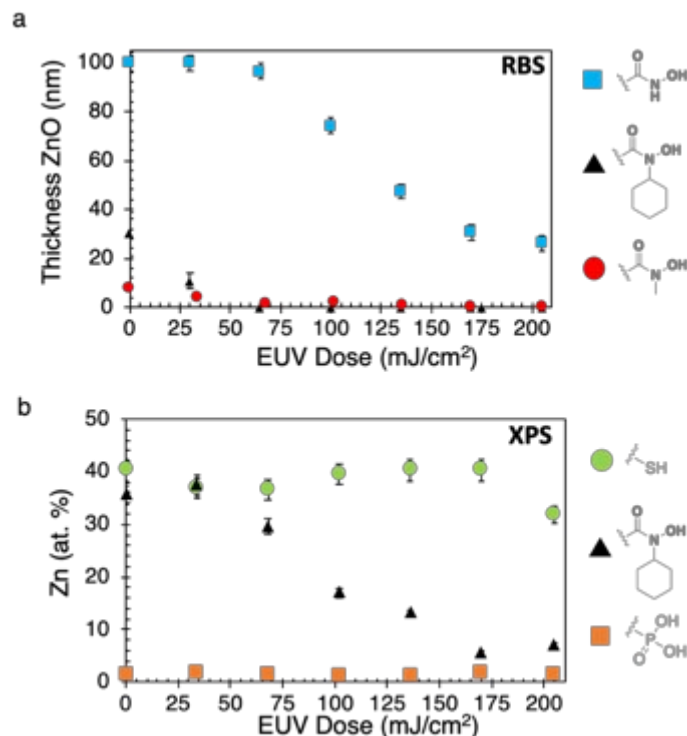
12

Figure 3: (**a**) ZnO film thickness produced from a set number of ALD cycles as measured by Rutherford Backscattering versus EUV dose of hydroxamic acid SAMs. ALD cycles used for SAM (**1**) 800, (**2**) 400, (**3**) 400 with a standard measurement error of 3% of the film thickness. (**b**) Surface concentration of Zn (at %) as measured by x-ray photoelectron spectroscopy after 400 ALD cycles for SAM produced from (**3**), octadecanethiol and octadecylphosphonic acid as a function of EUV irradiation dose. Standard error bars included in XPS results.

Inhibition Mechanism

To understand the photoinduced chemistry of the SAM film, near edge x-ray

absorption fine structure spectroscopy (NEXAFS) was used to characterize

two monolayer films composed of (**1**), before and after high dose electron

beam exposures (1 mC/cm^2), which maintain the same behavior as EUV

exposures after ALD development. Features in the carbon K-edge absorption

spectra were collected using a p-polarized beam incident at 20˚ and 75˚ with

respect to each substrate's plane, which provide information about the

13

surface coverage and orientation of carbon bonds. The feature at 293 eV for both samples is attributed to the C 1s → ☐* transitions from C-C single bonds, generally, oriented along the long axis of the octadecyl- chain. This assignment is supported by the higher intensity of the peak at 20˚ versus 75˚, suggesting the electric field vector at this glancing angle is resonating with the long axis of the side chain, normal to the substrate for both samples. There are two peaks at ca. 287-289 eV, whose intensity is also higher at 75˚ than 20˚, indicating resonance with these bonds is strongest when the incident electric field is parallel with the plane of the substrate. The lower energy peak at 287.8 eV is attributed to C 1s → ☐* transitions from the aliphatic C-H moieties whose bonding orientation is expected perpendicular to the octadecyl- chain.[44] After exposure C 1s → ☐* transitions decrease suggesting the concentration of aliphatic CH- moieties are lower, consistent with crosslinking of the SAM. Additionally, a slight increase in the peak at 285 eV after exposure is consistent with an increase in the concentration of C 1s → π* transitions from C=C bonds, further suggesting chemical crosslinking. The 75˚ – 20˚ difference spectra (**Figure 4b)** indicates dichroic features change considerably after exposure, where the unexposed sample exhibits features consistent with a perpendicular orientation of the SAM (e.g., overall perpendicular orientation of the C-C and C-H moieties) and the exposed sample a decrease in monolayer ordering/orientation is observed.[45] This disruption in ordering is, generally, correlated with chemical crosslinking and is observed in analogous materials

14

systems such as photo-crosslinked polyethylene.[46,47] FT-IR spectra after e-beam exposure shows CH-stretching at 2900 cm^{-1} decreases by ca. 30% in SAM film (**1**) and ca. 5% in SAM film (**2**) (**Figure S3**). In addition, peaks attributed to C-H bending at 1259 and 1310 cm^{-1} (consistent with reports of hydroxamic acid ligands)[48] were also observed to decrease after exposure. FT-IR then provides a consistent indication with NEXAFS that a decrease in C-H moieties occurs after exposure further suggesting the mechanism of increased inhibition is the result of SAM crosslinking.

NEXAFS spectra also provide an indication the chemical crosslinking induced by exposure is largely confined to the octadecyl- aliphatic tail group, as the O-K and N-K peaks attributed to the hydroxamic acid head groups do not exhibit a change in features (**Figure S6 & S7**).[49] Furthermore, DFT calculations suggest a photo-induced chemical reaction localized to the hydroxamic acid head group is not energetically favored (**Figure S8**), despite literature reports that describe the photosensitivity of several hydroxamic acid derivatives.[50]
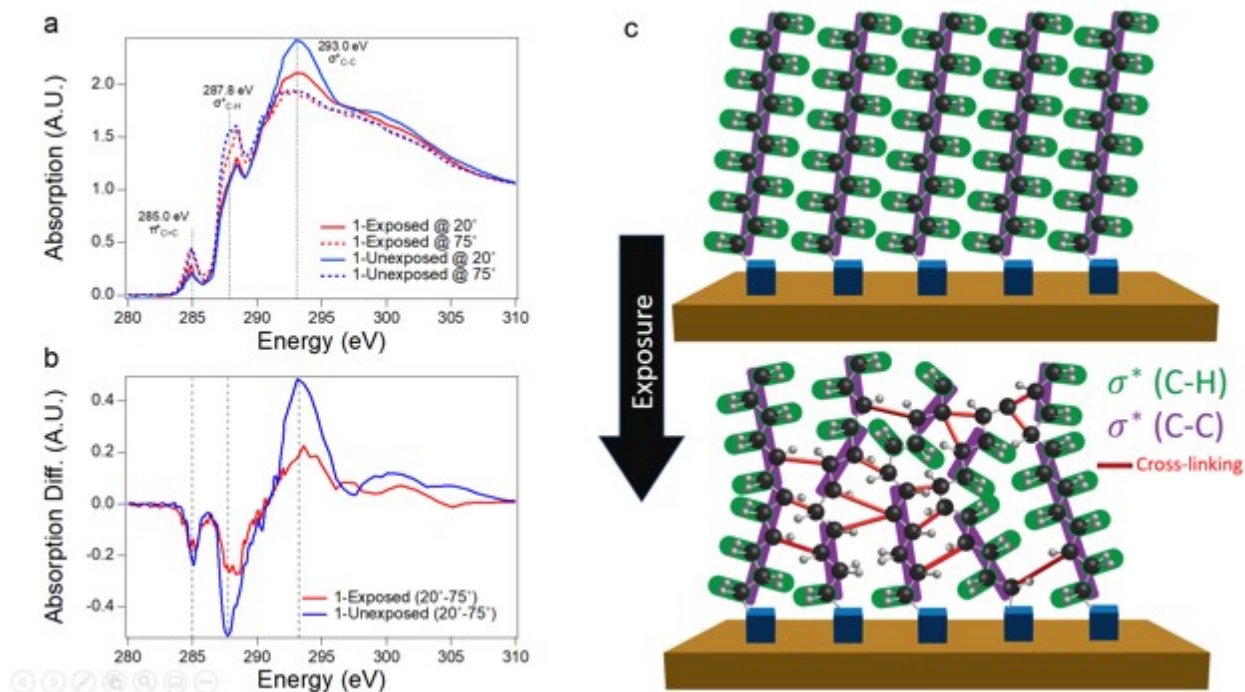
15

Figure 4: (**a**) Normalized angle-resolved p-polarized NEXAFS spectra across the carbon K-edge. (**b**) Difference spectra calculated from data shown in **a**. (**c**) Schematic representation of exposure-induced crosslinking mechanism.

Lithography Performance

Pattern generation with this materials system was first demonstrated with EUV exposures of (**1**) on a copper thin film followed by 700 ALD cycles of ZnO. This produced high contrast images with micron feature sizes observed by optical microscopy and AFM (**Figure 5**). AFM measurements exhibit a relationship between a trench depth as a function of EUV dose, where the highest EUV imaging dose gave the deepest trench (274 mJ cm^{-2}, trench depth ca. 15nm) and higher fidelity pattern features consistent with a more effective ALD barrier from irradiation induced chemistry. However, smaller features were not observed from this process, despite the critical dimensions of the exposure mask capable of generating nanometer scale
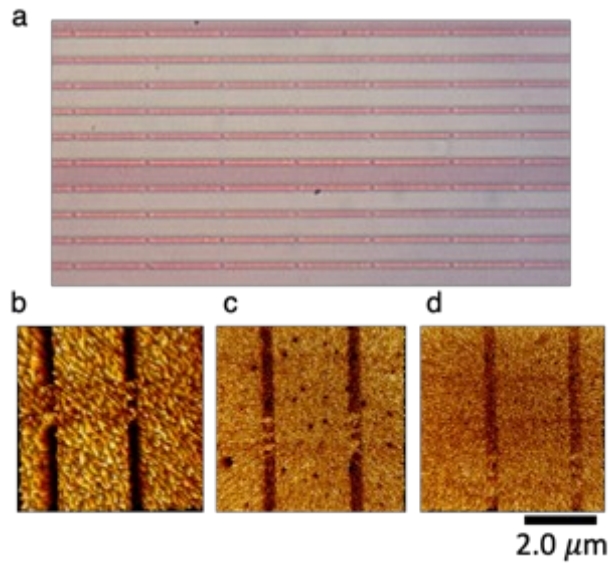
16

Figure 5: Patterns produced from the patternwise EUV irradiation of SAM produced from (**1**) after 600 ALD cycles of ZnO. (a) Optical image of line space pattern generated. AFM images of patterns as a function of EUV dose where the trench depth was observed to follow dose (b) at 274 mJ cm^{-2} 14.5nm (c) 180 mJ cm^{-2} 7.2 nm and (d) 118 mJ cm^{-2} 5.6nm. max. Z-scale 25nm.

features. The limiting resolution observed is not an inherent limitation of the material but may instead be the result of 700 ALD cycles where a film thickness of 35nm would be expected (based on open frame experiments, **Figure S1**) and lead to the lateral overgrowth of the ALD film to obscure nanometer size features.

In the development of EUV resists a number of material systems have been developed in e-beam and translated to EUV, provided the chemical reactions induced by the two irradiation sources (e-beam and EUV) are the same.[51,52]   This strategy provides the advantage of developing short loop experiments to optimize coating processes and ALD development conditions without having to resort to expensive EUV exposure tools and shift times.

17

Literature reports describe e-beam exposures as producing the same irradiation induced chemistry, in the crosslinking of aliphatic polymers as well as other SAM materials as observed in the EUV exposure of hydroxamic acid SAMs.[53,54] Gratifyingly, studies to screen the effects of e-beam exposures on hydroxamic acid SAMs produced the same behavior as EUV, where inhibition to ALD was enhanced. Direct write e-beam lithography targeted variable line widths from 1μm to 20nm using a dose array from 0.7-5 mC cm^{-2} as indicated. After e-beam lithography films were submitted to a specified number of ALD cycles. Initially, SAM generation of (**1**) on a copper thin films produced low contrast images after 600 cycles, where significant ALD nucleation sites were observed in e-beam exposed regions (**Figure 6**). While the patterning tone between E-beam EUV were the same (positive tone imaging) EUV did produce smoother features and lower line edge roughness on copper films coated. This difference was attributed to the absorption differences of the SAM and secondary electron generation that may induce more crosslinking in EUV than with e-beam exposures to provide better contrast between regions exposed vs. unexposed during the ALD process. To enhance pattern generation It was found that after exposure acetic acid (30s) could lift-off some portions of the unexposed SAM regions by dissolving the underlying copper oxide and lead to better contrast between the exposed and unexposed surfaces. Pattern fidelity improved but poor line edge roughness was still observed by AFM. This acetic acid was also very time sensitive where small deviations to the immersion time would

18

lead to blanket deposition of the ZnO, presumably from significant removal of the SAM material. The controlled introduction of surface roughness was found to provide further improvements to patterning resolution. Literature reports describe the impact of surface roughness using SAM inhibitors, where a material may be an effective inhibitor on substrates with low surface roughness. As roughness increases the inhibitors can exhibit almost complete loss of inhibition in severe cases.[55] In the context of hydroxamic acid SAMs, surface roughness may help enhance contrast in unexposed region of a film by reducing the delay in film deposition from the inherent inhibition properties of the SAM, though if roughness is too significant it may
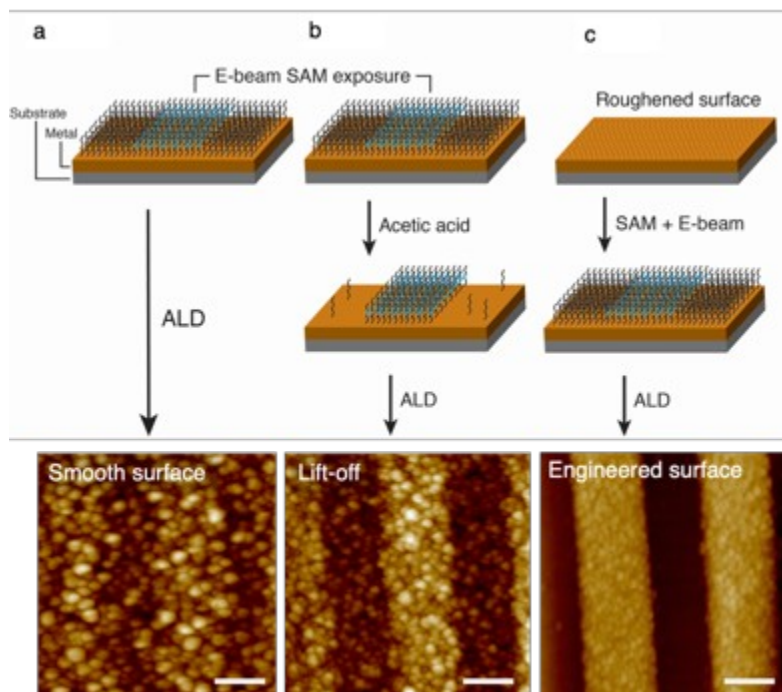
lead to a complete loss in inhibition. This method to improve contrast was demonstrated with the use of a ZnO underlayer and (**1**) was used to form a SAM on the surface.

19

Figure 6: Schematic of E-beam patterning of SAM (**1**) on a metal surface followed by 600 cycles of ZnO ALD to produce the resulting patterns as observed by AFM (scale bars 400nm, max Z-scale 20nm). (a) SAM on Cu thin film. (b) SAM on Cu thin film. After E-beam exposure unexposed SAM partially removed with acetic acid. (c) SAM on an engineered surface composed of ZnO providing increased surface roughness.

ALD ZnO produces a polycrystalline film on silicon using a standard ALD recipe (see SI for details) where typical grain sizes are ca. 10nm. AFM characterization of the RMS surface roughness for a 10nm ZnO thin film was 1.2nm, compared to a thermally evaporated Cu thin film which exhibits an RMS roughness of 0.5nm.   E-beam lithography was used to generate exposure patterns followed by ALD development that exhibited better control over feature generation where AFM shows a significant reduction in the frequency of ALD nucleation sites in the exposed regions of the film (**Figure 6**). Pattern resolution and fidelity was also dramatically improved with this strategy where features as small as 50nm could be generated (**Figure 7**). To further characterize the effects of this underlayer on exposure induced inhibition open frame   EUV exposures were also conducted using (**1**) on a ZnO surface. With this underlayer less ALD cycles were required for pattern development where the number of cycles were reduced from 600 (on copper) to 400 cycles (on ALD ZnO) and consistent with e-beam pattern generation. The controlled introduction of surface roughness therefore presents an additional strategy for controlling the patterning and area selective deposition using hydroxamic acid SAMs.

NEXAFS was used to confirm the change in contrast was the result of increased surface roughness and not a modification to the SAM ordering,

20

which may impact the irradiation induced chemistry. The orientation of a crystalline SAM can be inferred from angle dependence of NEXAFS spectra[56] and, generally, requires two extreme angles to reconstruct this dependence.[57] Comparing the difference spectra between either a smooth surface or the roughened surface provides a qualitative indication of whether SAM ordering is modified. (**1**) on a roughened or smooth surface, exhibits substantially equivalent difference spectra, an indication that SAM ordering is not significantly affected (**Figure S14**).[58] Furthermore, the individual spectra at 20, 60 and 80° show similar features and trends, though a change in peak intensity at 293 eV at 40° is observed, for ZnO and is likely a result of film roughness.

The effect of increased underlayer absorbance in EUV or e-beam was also examined to determine if this could be another method to adjust contrast in this patterning system using a SAM produced from (**1**) deposited on a higher EUV absorbing film that was explored with ALD generated TiO_2.[59] In comparison to Cu the TiO_2 film exhibits a similar RMS roughness but has a

21
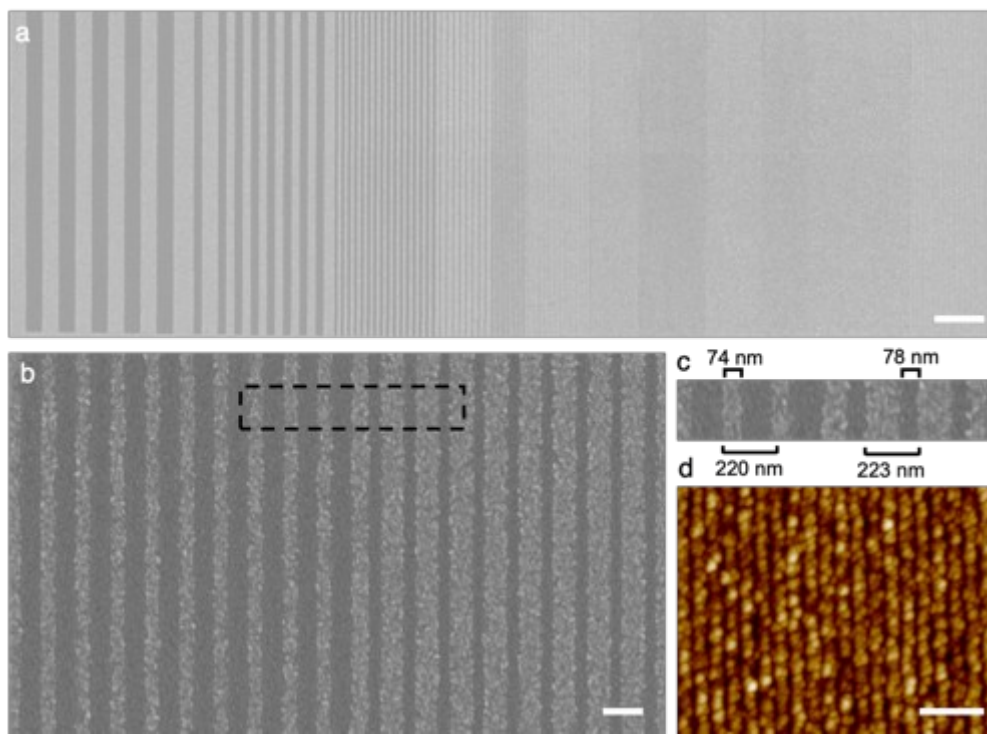
higher EUV absorbance than Cu. Presumably, if the higher absorbance provides more secondary electrons this could be anticipated to provide more crosslinking events and therefore better contrast. However, after EUV exposures no reduction in the number of ALD cycles required for development was observed (compared to **1** on Cu films) (**Figure S13**).

Figure 7: E-beam pattern generated from SAM (1) on a ZnO surface after 600 cycles of ZnO ALD. (a) Top down SEM image, scale bar 3µm. (b) Top down SEM of variable line space pattern, scale bar 200nm. Inset highlighted. (c) Inset with dimensions measured of pattern widths. (d) AFM image of smallest line patterns observed measured at 50nm width. AFM scale bar 400nm, max. z-scale 17nm.

Hydroxamic acids can also be deposited in a manner that favors multilayer formation by the immersion of a cleaned metal oxide surface in a solution of (**1**) and rinsing with a non-interacting solvent that engages intermolecular hydrogen bonds between head groups. While difficult to control multilayer formation, multilayer regions could be generated in an otherwise monolayer film. E-beam patterning and ALD development of this multilayer exhibited the reverse imaging tone, negative tone, compared to monolayers of (**1**) (**Figure S15**). Consistent with reports of other disordered monolayer systems such as trichlorosilanes, which can readily generate multilayer films which upon e-beam exposures lead to oxidation of the multilayer creating polar oxygen containing moieties that promote ALD growth and therefore lead to the opposite imaging tone where ALD film deposition occurs more readily in the exposed regions of the film (**Figure S16**).[60,61,62,63] The formation of hydroxamic acid multi-layers may also lead to the same behavior where oxidation reactions are favored from exposure. The

22

difference in this irradiation induced chemistry would be consistent with the behavior of aliphatic polymers such as polyethylene, where films have both crystalline and amorphous domains. e-beam exposure of polyethylene films lead to first the formation of radicals from the homolysis of C-H bonds that leads to interchain crosslinking in the crystalline domains and oxidation in the amorphous regions. This is attributed to a difference in the ability for oxygen diffusion to occur in the amorphous domains that more readily reacts with the exposure induced radicals to form of polar moieties (e.g., aldehydes, carboxylic acid and hydroxyl groups) and the denser packing of crystalline regions have chain orientations that favors intermolecular crosslinking.[64]

Self-aligned Inhibitor & Patterning

The patterning capability of hydroxamic acid SAMs combined with their property to selectively attach to metal surfaces (e.g., self-alignment) offers an additional capability for an ASD process. The combination of these functionalities enables an additional level of control over pattern formation, rather than the reflection of an underlying pre-pattern as most other ASD processes, generally, offer. Self-alignment refers to the ability of a material to be selectively deposited on one surface of a pattern, such as the surface of a metal or metal oxide surface, without depositing on another, allowing the material to be deposited without patterning and therefore without the need for alignment. A patterned coplanar surface consisting of copper lines and a silicon spaces was used to demonstrate this (**Figure S17**). (**1**) was

selectively deposited on the Cu portion of the pattern forming a SAM which then underwent pattern-wise e-beam exposure at various doses to write two distinct patterns: (i) the Latin character 'B' and (ii) a square border that contained three smaller squares and a rectangle (**Figure 8**).   The exposed SAMs were developed with 500 ALD cycles and show high-fidelity relief images with significant dependence on e-beam dose. The differences in film thickness as a function of e-beam dose were characterized with AFM using the pattern 'B' where differences in film thickness increased from 2-5 mC cm^{-2}. At the highest doses (4 & 5 mC cm^{-2}) the difference in height between the exposed and unexposed regions of the pattern 'B' were measured at 24 nm and decreased as dose was further reduced to 14 nm with 3 mC cm^{-2} to and 10nm with 2 mC cm^{-2}. At the highest dose of 5 mC cm^{-2} relief images of a square border were also generated showing the ability to generate arbitrary features with this technique.
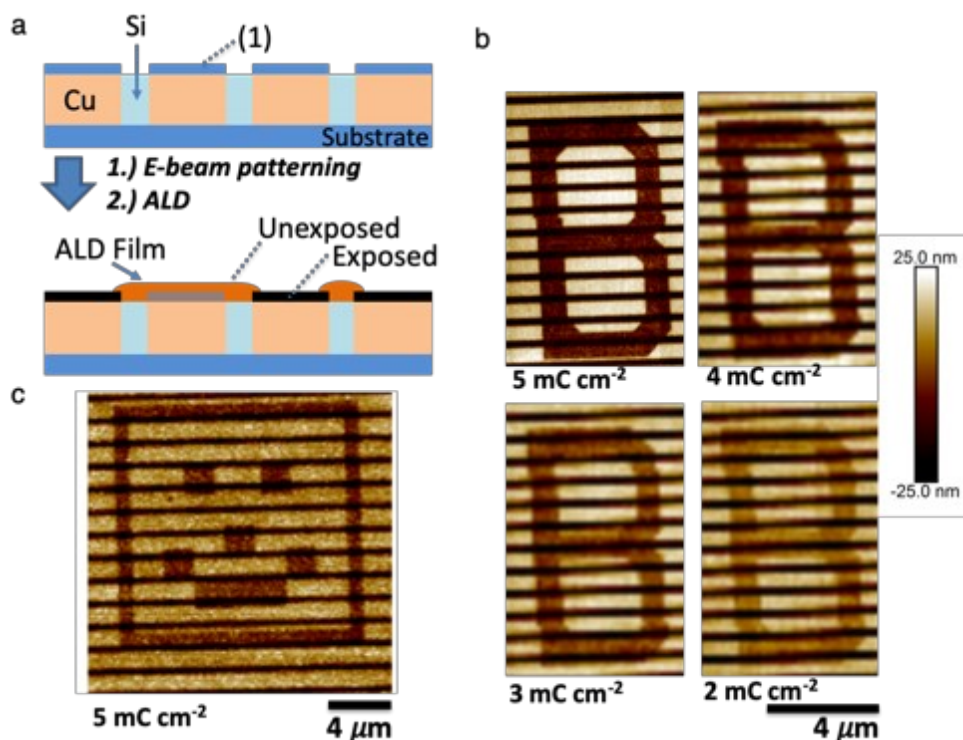
Figure 8: (**a**) Schematic process flow involving the use of SAM produced from (**1**) on a pre-patterned surface followed by the deposition behavior after e-beam patterning and ALD. (**b**) AFM images of a patterned Latin character 'B' as a function of e-beam dose. (**c**) AFM relief image produced after e-beam exposure and ALD of concentric square and rectangle patterns.

Conclusions

The combination of a patternable hydroxamic acid based monolayers with

ASD provides an example of an additive approach to lithography, where a

pattern is developed by an ALD step to form a relief image where

controllable patterns as small as 50nm could be generated. In this materials

system several variables were found to provide the ability to tune contrast

and improve imaging resolution. Reducing intramolecular interactions

between monolayer components were found to enhance inhibition contrast

and reduce exposure dose and by using surfaces with some roughness an

25

improvement in pattern definition could be achieved. These parameters may be further tuned and optimize to achieve greater resolution and pattern definition, and there may be additional material characteristics that can be introduced for further improvements to dose and contrast.   Furthermore, the ability of these materials to self-align and form a SAM on a pre-patterned surface provides another tool to ASD where a blocking mask can be used to crosslink the SAM and grow a film on both the dielectric and unexposed portion of the metal surface. As device dimensions continue to shrink, surfaces and interfaces become increasingly significant and dominate performance in the single nanometer regime. This demonstration focused on the combination of chemical patterning and ASD has implications in device fabrication and the element of chemical patterning may be exploited in future selective surface modifications, to generate the pattern-wise adhesion of reagents for catalysis,[65] antibodies for biosensors[66] or produce organic electronic devices.[67]
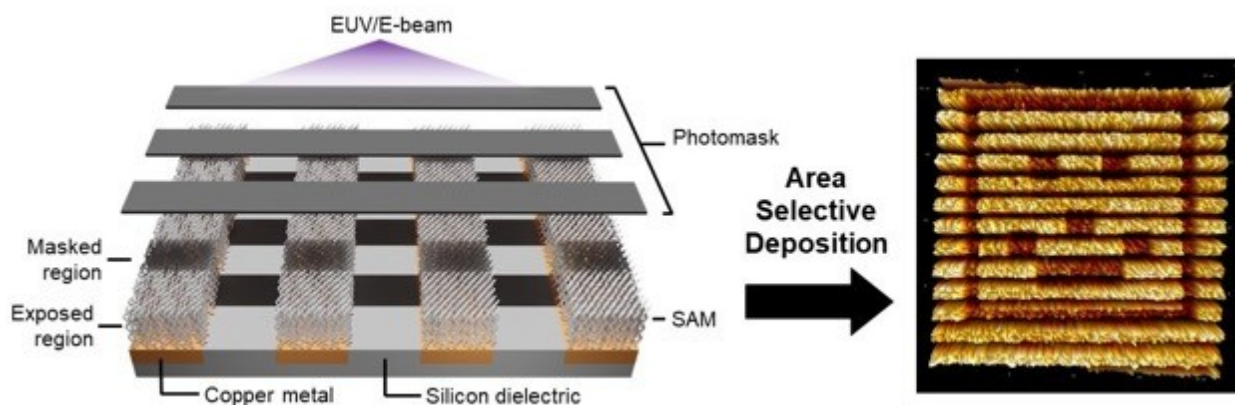
Supporting Information

Experimental procedures for synthesis of monolayers, characterization, atomic layer deposition and extreme ultraviolet exposures. Additional characterization data – Nitrogen N-K NEXAFS, Oxygen K-Edge NEXAFS, XPS, static water contact angles, microscopy images of EUV and e-beam exposures of SAMs after ALD & Rutherford backscattering — is also included.

Acknowledgements

26

Graphical Abstract

TOC Caption: Self-aligning photo-responsive self-assembled monolayers undergo chemical crosslinking in response to irradiation. This behavior and the design of monolayer components were exploited in a lithographic system based on area selective deposition, an additive approach to lithography in contrast with traditional subtractive methods.

27

References

[1] Park, S.H.; Kang, Y.J. ; Majd., S. A Review of Patterned Organic Bioelectronic Materials and their Biomedical Applications. *Adv. Mater.* **2015**, *27,* 7583-7619.

[2] Zhu, S.; Meng, Q.; Wang, L.; Zhang, J.; Song, Y.; Jin, H.; Zhang, K.; Sun, H.; Wang, H.; Yang., B. Highly Photoluminescent Carbon Dots for Multicolor Patterning, Sensors and Bioimaging. *Angew. Chem. Int. Ed.* **2013**, *52*, 3953-3957.

[3] Khan, S. ; Lorenzelli, L. ; Dahiya., R.S. Technologies for Printing Sensors and Electronics Over Large Flexible Substrates: A Review. *IEEE Sensors Journal* **2015**, *15(6)*, 3164-3185.

[4] Ameloot, R.; Gobechiya, E.; Uji-I, H.; Martens, J.A.; Hofkens, J.; Alaerts, L.; Sels, B.F.; De Vos., D.E. Direct Patterning of Oriented Metal-Organic Framework Crystals via Control Over Crystallization Kinetics in Clear Precursor Solutions. *Adv. Mater.* **2010**, *22*, 2685-2688.

[5] Wagner, C.; Bacelar, J.; Harned, N.; Loopstra, E.; Hendriks, S.; Jong, I.; Kuerz, P.; Levasier, L.; Kerkhof, M.; Lowisch, M.; Meiling, H.; Ockwell, D.; Peeters, R.; Setten, E.; Stoeldraijer, J.; Young, S.; Zimmerman, J.; Kool, R. EUV Lithography at Chipmakers has Started: Performance Validation of ASML's NXE:3100. *Proc. SPIE 7969 Extreme Ultraviolet (EUV) Lithography II* **2011**, 79691F.

[6] Kaisti, M. Detection Principles of Biological and Chemical FET Sensors. *Biosens. and Bioelect.* **2017**, *98*, 437-448.

[7] Kumar, N.; Parajuli, O.; Gupta, A.; Hahm, J. Elucidation of Protein Adsorption Behavior on Polymer Surfaces: Toward High-Density, High-Payload Protein Templates. *Langmuir* **2008**, *24*, 2688-2694.

[8] Marruecos, D.F.; Kienle, D.F.; Kaar, J.L.; Schwartz, D.K. Grafting Density Impacts Local Nanoscale Hydrophobicity in Poly(ethylene glycol) Brushes. *ACS Macro Lett.* **2018**, *7*, 498-503.

[9] Reddy, B.; Salm, E.; Bahir, R. Electrical Chips for Biological Point-of-Care Detection. *Annu. Rev. Biomed. Eng.* **2016**, *18*, 329-355.

[10] Brichon, P.; Despiau-Pujo, E.; Joubert, O. MD Simulations of Low Energy Clx+ Ions Interaction with Ultrathin Silicon Layers for Advanced Etch Processes. *J. Vac. Sci Technol. A* **2014**, *32(3)*, 021301.

[11] Tao, Q.; Jurisch, G.; Takoudis, C. Selective Atomic Layer Deposition of HfO_2 on Copper Patterned Silicon Substrates. *Appl. Phys. Lett.* **2010**, *96*, 192105.

[12] George, S.M.; Yoon, B.; Dameron, A.A. Surface Chemistry for Molecular Layer Deposition of Organic and Hybrid Organic-Inorganic Polymers. *Polymers. Acc. Chem. Res.* **2009**, *42(4)*, 498-508.

[13] Mackus, A.J.M.; Merkx, M.J.M.; Kessels, W.M.M. From the Bottom-Up: Toward Area-Selective Atomic Layer Deposition with High Selectivity. *Chem. of Mater.* **2019**, *31(1)*, 2–12.

[14] Stevens, E.; Tomczak, Y.; Chan, B.T.; Sanchez, E.A.; Parsons, G.N.; Delabie, A. Area-Selective Atomic Layer Deposition of TiN, TiO_2, and HfO_2 on Silicon Nitride with inhibition on Amorphous Carbon. *Chem. Mater.* **2018**, *30(10)*, 3223-3232.

[15] Atanasov, S.E.; Kalanyan, B.; Parsons, G.N. Inherent Substrate-dependent Growth Initiation and Selective-Area Atomic Layer Deposition of TiO2 using "Water-Free" Metal-Halide/Metal Alkoxide Reactants. *J. Vac. Sci. Technol. A* **2016**, *34(1)*, 01A148.

[16] Färm, E.; Kemell, M.; Ritala, M.; Leskelä, M. Selective-Area Atomic Layer Deposition Using Poly(methyl methacrylate) Films as Mask Layers. *J. Phys. Chem. C* **2008**, *112*, 15791-15795.

[17] Zyulkov, I.; Voronina, E.; Krishtab, M.; Voloshin, D.; Chan, B.T.; Mankelevich, Y.; Rakhimova, T.; e, S.; De Gendt, S. Area-Selective Ru ALD by Amorphous Carbon Modification using H-Plasma: from Atomistic Modeling to Full Wafer Process Integration. *Mater. Adv.* **2020**, *1*, 3049-3057.

[18] Stevens, E.; Tomczak, Y.; Chan, B.T.; Sanchez, E.A.; Parsons, G.N.; Delabie, A. Area-Selective Atomic Layer Deposition of TiN, TiO2, and HfO2 on Silicon Nitride with Inhibition on Amorphous Carbon. *Chem. Mater.* **2018**, *30(10)*, 3223-3232.

[19] George, S.M.; Yoon, B.; Dameron, A.A. Surface Chemistry for Molecular Layer Deposition of Organic and Hybrid Organic-Inorganic Polymers. *Poly. Acc. Chem. Res.* **2009**, *42(4)*, 498-508.

[20] Zyulkov, I.; Madhiwala, V.; Voronina, E.; Snelgrove, M.; Bogan, J.; O'Conner, R.; De Gendt, S.; Armini, S. Area-Selective ALD of Ru on Nanometer-Scale Cu Lines through Dimerization of Amino-Functionalized Alkoxy Silane Passivation Films. *ACS Appl. Mater. Interfaces* **2020**, *12(4)*, 4678-4688.

[21] Jiang, X.; Bent, S.F. Area-Selective Atomic Layer Deposition of Platinum on YSZ Substrates Using Microcontact Printed SAMS. *J. Electrochem. Soc.* **2007**, *154(12)*, D648-D656.

[22] Hashemi, F.S.M.; Bent, S.F. Sequential Regeneration of Self-Assembled Monolayers for Highly Selective Atomic Layer Deposition. *Adv. Mater. Inter.* **2016**, *3(21)*, 1600464.

[23] Chen, R.; Bent, S.F. Highly Stable Monolayer Resists for Atomic Layer Deposition on Germanium and Silicon. *Chem. Mater.* **2006**, *18*, 3733-3741.

[24] Mameli, A.; Karasulu, B.; Verheijen, M.A.; Barcones, B.; Macco, B.; Mackus, A.J.M.; Kessels, W.M.M.; Roozeboom, F. Area-Selective Atomic Layer Deposition of ZnO by Area Activation Using Electron Beam-Induced Deposition. *Chem. Mater.* **2019**, *31(4)*, 1250–1257.

[25] Mettry, M.; Hess, A.E.; Goetting, I.; Arellano, N.; Friz, A.; Tek, A.T.; Wojtecki, R. Extending the Compositional Diversity of Films in Area Selective Atomic Layer Deposition through Chemical Functionalities. *J. Vac. Sci. Technol. A* **2019**, *37*, 020923.

[26] Wojtecki, R.; Mettry, M.; Fine Nathel, N.F.; Friz, A.; De Silva, A.; Arellano, N.; Shobha, H. Fifteen Nanometer Resolved Patterns in Selective Area Atomic Layer Deposition – Defectivity Reduction by Monolayer Design. *ACS Appl. Mater. Interfaces* **2018**, *10*, 38630–38637.

[27] Bobb-Semple, D.; Nardi, K.L.; Draeger, N.; Hausmann, D.M.; Bent, S.F. Area-Selective Atomic Layer Deposition Assisted by Self-Assembled Monolayers: A Comparison of Cu, Co, W, and Ru. *Chem. Mater.* **2019**, *31(5)*, 1635-1645.

[28] Ulman, A. Formation and Structure of Self-Assembled Monolayers. *Chem. Rev.* **1996**, *96*, 1533-1554.

[29] Hashemi, F.S.M.; Prasittichai, C.; Bent, S.F. A New Resist for Area Selective Atomic and Molecular Layer Deposition on Metal-Dielectric Patterns. *J. Phys. Chem. C* **2014**, *118*, 10957-10962.

[30] Chen, R.; Kim, H.; McIntyre, P.C.; Bent, S.F. Investigation of Self-Assembled Monolayer Resists for Hafnium Dioxide Atomic Layer Deposition. *Chem. Mater.* **2005**, *17(3)*, 536-544.

[31] Prasittichai, C.; Pickrahn, K.L.; Hashemi, F.S.M.; Bergsman, D.S.; Bent, S.F. Improving Area-Selective Molecular Layer Deposition by Selective SAM Removal. *Appl. Mater. Interfaces* **2014**, *6(20)*, 17831-17836.

[32][] Parsons, G.N. Functional Model for Analysis of ALD Nucleation and Quantification of Area-Selective Deposition. *J. Vac. Sci. & Technol. A* **2019**, *37(2)*, 020911.

[33][] Pattison, T.G.; Hess, A.E.; Arellano, N.; Lanzillo, N.; Nguyen, S.; Bui, H.; Rettner, C.; Truong, H.; Friz, A.; Topura, T.; Fong, A.; Hughes, B.; Tek, A.T.; DeSilva, A.; Miller, R.D.; Qiao, G.G.; Wojtecki, R.J. Surface Initiated Polymer Thin Films for the Area Selective Deposition and Etching of Metal Oxides. *ACS Nano* **2020**, *14(4)*, 4276-4288.

[34][] Johnson, R.W.; Hultqvist, A.; Bent, S.F. A Brief Review of Atomic Layer Deposition: from Fundamentals to Applications. *Materials Today* **2014**, *17(5)*, 236–246.

[35][] Leskela, M.; Ritala, M. Atomic Layer Deposition (ALD): from Precursors to Thin Film Structures. *Thin Solid Films* **2002**, *409*, 138-146.

[36][] Kim, H.; Oh, I.K. Review of Plasma-Enhanced Atomic Layer Deposition: Technical Enabler of Nanoscale Deviation Fabrication. *Jpn. J. Appl. Phys.* **2014**, *53*, 03DA01-8.

[37][] Reichmanis, E.; Houlihan, F.M.; Nalamasu, O.; Neenan, T.X. Chemical Amplification Mechanisms for Microlithography. *Chem. Mater.* **1991**, *3*, 394-407.

[38][] Folkers, J.P.; Gorman, C.B.; Laibinis, P.E.; Buchholz, S.; Nuzzo, R.G.; Whitesides, G.M. Self-Assembled Monolayers of Long-Chain Hydroxamic Acids on the Native Oxides of Metals. *Langmuir* **1995**, *11*, 813-824.

[39][] Dubey, M.; Weidner, T.; Gamble, L.J.; Castner, D.G. Structure and Order of Phosphonic Acid-Based Self-Assembled Monolayers on Si(100). *Langmuir* **2010**, *26(18)*, 14747-14754.

[40][] Jeynes, C.; Colaux. J.L. Thin Film Depth Profiling by Ion Beam Analysis. *Analyst* **2016**, *141*, 5944-5985.

[41][] J. Drelich, K.L. Mittal, Atomic Force Microscopy in Adhesion Studies, CRC Press, Taylor and Francis Group **2005**, New York.

[42][] Wen, J.; Li, W.; Chen, S.; Ma, J. Simulations of Molecular Self-Assembled Monolayers on Surfaces: Packing Structures, Formation Processes and Functions Tuned by Intermolecular and Interfacial Interactions. *Phys. Chem. Chem. Phys.* **2016**, *18*, 22757-22771.

[43][] Pipek, J.; Mezey, P.G. A fast intrinsic localization procedure applicable for ab initio and semiempirical linear combination of atomic orbital wave functions. *J. of Chem. Phys.* **1989**, *90 (9)*, 4916-4920.

[44][] Bagus, P.S.; Weiss, K.; Schertel, A.; Woll, C.; Braun, W.; Hellwig, C.; Jung, C. Identification of Transitions into Rydberg States in the X-ray Absorption Spectra of Condensed Long-Chain Alkanes. *Chem. Phys. Lett.* **1996**, *248(3-4)*, 129-135.

[45][] Latham, K.G.; Simone, M.I.; Dose, W.M.; Allen, J.A.; Donne, S.W. Synchrotron Based NEXAFS Study on Nitrogen Doped Hydrothermal Carbon: Insights into Surface Functionalities and Formation Mechanisms. *Carbon* **2017**, *114*, 566-578.

[46][] Charlesby, A.; Callaghan., L. Crystallinity Changes in Irradiated Polyethylenes. *J. of Phys. and Chem. Sol.* **1958**, *4(4)*, 306-314.

[47][] Ries, M.D.; Pruitt., L. Effect of Cross-Linking on the Microstructure and Mechanical Properties of Ultra-High Molecular Weight Polyethylene. *Clin. Orthop. Relat. Res.* **2005**, *440*, 149-156.

[48][] Yang, J.; Bremer, P.J.; Lamont, I.L.; McQuillan, A.J. Infrared Spectroscopic Studies of Siderophore-Related Hydroxamic Acid Ligands Adsorbed on Titanium

Dioxide. *Langmuir* **2006**, *22*, 10109-10117.

[49] Watts, B.; Thomsen, L.; Dastoor, P.C. Methods in Carbon K-edge NEXAFS: Experiment and Analysis. *J. Elect. Spect. and Relat. Phenom.* **2006**, *151(2),* 105-120.

[50] Lipczynska-Kochany, E. Photochemistry of Hydroxamic Acids and Derivatives. *Chem. Rev.* **1991**, *91*, 477-491.

[51] Oyama, T.G.; Oshima, A.; Tagawa, S. Estimation of Resist Sensitivity for Extreme Ultraviolet Lithography using an Electron Beam. *AIP Adv.* **2016**, *6*, 085210.

[52] Bhattarai, S.; Neureuther, A.R.; Naulleau, P.P. Study of Shot Noise in Photoresists for Extreme Ultraviolet Lithography through Comparative Analysis of Line Edge Roughness in Electron Beam and Extreme Ultraviolet Lithography. *J. Vac. Soc.* & Tech. B. **2017**, *35*, 061602.

[53] Tretinnikov, O.N.; Ogata, S.; Ikada, Y. Surface Crosslinking of Polyethylene by Electron Beam Irradiation in Air. *Polymer* 1998, *39(24)*, 6115-6120.

[54] She, Z.; DiFalco, A.; Hahner, G.; Buck, B. Electron-beam Patterned Self-Assembled Monolayers as Templates for Cu Electrodeposition and Lift-off. *Beilstein J. Nanotechnol.* **2012**, *3*, 101-113.

[55] Chockalingam, M.; Darwish, N.; Le Saux, G.; Gooding, J.J. Importance of the Indium Tin Oxide Substrate on the Quality of Self-Assembled Monolayers Formed from Organophosphonic Acids. *Langmuir* **2011**, *27*, 2545–2552.

[56] Kondoh, H.; Saito, N.; Matsui, F.; Yokoyama, T.; Ohta, T.; Kuroda, H. Structure of Alkanethiolate Monolayers on Cu(100): Self-Assembly on the Four-Fold-Symmetry Surface. *J. Phys. Chem. B* **2001**, *105(51)*, 12870-12878.

[57] Stöhr, J.; Outka, D. A. Determination of Molecular Orientations on Surfaces From the Angular Dependence of Near-Edge X-ray-Absorption Fine-Structure Spectra. *Physical Review B* **1987**, *36(15)*, 7891-7905.

[58] Semple, D.B.; Zeng, L.; Cordova, I.; Bersman, D.S.; Nordlund, D.; Bent, S.F. Substrate-Dependent Study of Chain Orientation and Order in Alkylphosphonic Acid Self-Assembled Monolayers for ALD Blocking. *Langmuir* **2020**, *36(43),* 12849-12857.

[59] Li, L.; Liu, X.; Pal, S.; Wang, S.; Ober, C.K.; Giannelis, E.P. Extreme Ultraviolet Resist Materials for Sub-7nm Patterning. *Chem. Soc. Rev.* **2017**, *46*, 4855-4866.

[60] Rozlosnik, N.; Gerstenberk, M.C.; Larsen, N.B. Effect of Solvents and Concentration on the Formation of a Self-Assembled Monolayer of Octadecylsiloxane on Silicon (001). *Langmuir* **2003**, *19(4)*, 1182-1188.

[61] Huang, J.; Lee, M.; Lucero, A.; Cheng, L.; Kim, J. Area-Selective ALD of TiO_2 Nanolines with Electron-Beam Lithography. *J. Phys. Chem. C* **2014**, *118*, 23306-23312.

[62] Seshadri, K.; Froyd, K.; Parikh, A.N.; Allara, D.L.; Lercel, M.J.; Craighead, H.G. Electron-Beam-Induced Damage in Self-Assembled Monolayers. *J. Phys. Chem.* **1996**, *100(39)*, 15900-15909.

[63] Ulman, A. Formation and Structure of Self-Assembled Monolayers. *Chem. Rev.* **1996**, *96,* 1533-1554.

[64] Michaels, A. S.; Bixler, H. J. Solubility of Gases in Polyethylene. *J. Polym. Sci.* **1961**, *50(393),* 393-412.

[65] Cote, A.S.; Delgass, W.N.; Ramkrishna, D. Investigation of Spatially Patterned Catalytic Reactors. *Chem. Eng. Sci.* **1999**, *54(13-14)*, 2627-2635.

[66][] Koespel, J.T.; Murphy, W.L. Patterned Self-Assembled Monolayers: Efficient, Chemically Defined Tools for Cell Biology. *Chem. Bio. Chem.* **2012**, *13(12)*, 1717-1724.

[67][] Biswas, S.; Shalev, O.; Shtein, M. Thin-Film Growth and Patterning Techniques for Small Molecular Organic Compounds used in Optoelectronic Device Applications. *Annu. Rev. Chem. Biomol. Eng.* **2013**, *4*, 289-317.